Computers and Geotechnics 138 (2021) 104322

Contents lists available at ScienceDirect

Computers and Geotechnics

journal homepage: www.elsevier.com/locate/compgeo

Random finite element analysis of backward erosion piping

B.A. Robbins [a,b,*], D.V. Griffiths [b], Gordon A. Fenton [c]

[a] U.S. Army Corps of Engineers, 12596 W. Bayaud Avenue, Lakewood, CO 80236, USA
[b] Department of Civil and Environmental Engineering, Colorado School of Mines, 1500 Illinois Street, Golden, CO 80401, USA
[c] Department of Engineering Mathematics, Dalhousie University, Halifax, NS, Canada

ARTICLE INFO

Keywords:
Internal erosion
Backward erosion piping
Random finite element method

ABSTRACT

Backward erosion piping (BEP) is a type of internal erosion that threatens the integrity of dams and levees. BEP has been shown to be highly sensitive to spatial variations in soil properties; however, there are presently no assessment methods that permit incorporating spatial variation in soil properties into BEP analysis. The Random Finite Element Method (RFEM) is a numerical approach for incorporating spatially variable properties into finite element analysis. In this study, an RFEM approach to simulating BEP was developed to assess pipe progression through variable soils. The soil hydraulic conductivity and critical hydraulic gradient for pipe progression were treated as log-normal random variables. Analyses were conducted for a range of hydraulic conductivity and critical gradient random fields with varied spatial correlation lengths, distribution parameters, and field correlations. Results indicate that the probability of failure increases with increasing spatial correlation length. Additionally, increased variance in soil permeability was shown to increase the probability of failure for large correlation lengths and decrease the probability of failure for short correlation lengths. Regardless of correlation length, increasing values of the mean critical hydraulic gradient led to decreased failure probabilities, and increasing values of critical hydraulic gradient variance led to increased failure probabilities.

1. Introduction

Backward erosion piping (BEP) is a type of internal erosion that threatens the integrity of water retaining structures such as dams and levees. BEP occurs when small, shallow erosion channels progress upstream through erodible foundation sands beneath a dam or levee as depicted in Fig. 1. The erosion initiates through an unfiltered seepage exit such as a hole through the confining layer or simply an exposed sand layer (e.g., in the bottom of a ditch). Once the erosion initiates, the erosion pipe can gradually progress upstream if seepage flow through the pipe tip is sufficient to cause further erosion. The erosion pipe will progress through the sand below the clay cover layer as the clay forms a cohesive roof over the erosion channel which allows it to remain open. If the erosion pipe is able to progress to the upstream boundary, the flow through the pipe increases rapidly causing the pipe to enlarge and potentially collapse the structure. For the interested reader, an excellent description of the physical process of backward erosion piping is provided in Van Beek et al. (2010) and Van Beek (2015).

Historically speaking, BEP has been a leading cause of failures for both dams and levees (Foster et al. 2000, Richards and Reddy 2007, Baker 2018, Van Beek et al. 2013). It has long been recognized that BEP is an issue of concern in the design and construction of dams and levees (Clibborn, 1902; Bligh, 1910; Lane, 1935; Terzaghi and Peck, 1948). Early design approaches against BEP used empirical approaches based on failure case histories to develop suggested design guidelines for dams (Bligh, 1910; Lane, 1935). From a modern perspective, the shortcomings of these approaches lie in (1) the limited information available for the case histories, (2) the fact that there are significant design differences between the early 20th century designs and designs of today, and (3) the use of failures caused by all types of internal erosion in the development of the empirical methods (not specifically backward erosion piping). Because of these issues, significant research has been conducted attempting to develop mechanics-based predictive methods for analysis of BEP. A thorough understanding of the physical processes involved in BEP has been developed over the years through various experimental investigations (e.g., Peitrus, 1981; De Wit, 1984; Hanses, 1985; Townsend et al., 1988; Van Beek et al., 2010; Van Beek, 2015; Allan, 2018; Robbins et al., 2018; Vandenboer, 2019). With reference to the numbers in Fig. 1, the BEP process involves (1) flow through porous media; (2) initiation of erosion through grain detachment and transport at an unfiltered seepage exit; (3) highly concentrated seepage near the pipe

* Corresponding author.
E-mail address: Bryant.a.robbins@usace.army.mil (B.A. Robbins).

https://doi.org/10.1016/j.compgeo.2021.104322

Available online 8 July 2021
0266-352X/Published by Elsevier Ltd.

Nomenclature

a	depth of the erosion pipe (m)
A	cross sectional area of the erosion pipe (m^2)
d_{50}	median grain size of sand (m)
D_H	hydraulic diameter of the erosion pipe (m)
f	Darcy–Weisbach friction factor
g	gravitational acceleration (m/s^2)
h	piezometric head (m)
$\{H\}$	vector of nodal heads (m)
$(H/L)_{cr}$	critical value of the average hydraulic gradient for BEP progression through the domain
i_{cr}	critical hydraulic gradient magnitude for pipe progression
i_h	magnitude of the hydraulic gradient vector
k	hydraulic conductivity (m/s)
$[k_e]$	local element conductivity matrix (m/s)
k_x	hydraulic conductivity in the x-direction (m/s)
k_y	hydraulic conductivity in the y-direction (m/s)
k_{pL}	equivalent hydraulic conductivity for laminar flow in the erosion pipe (m/s)
$[K_e]$	global conductivity matrix (m/s)
L	length of the analysis domain in the direction of piping (m)
N_i	finite element shape functions
P	wetted perimeter of the erosion pipe (m)
$\{Q\}$	vector of net nodal flowrates (m^2/s)
V	average velocity in the erosion pipe (m/s)
W	width of the analysis domain perpendicular to the direction of piping (m)
w	width of the erosion pipe (m)
x	position in the x-direction (m)
x_i	x-coordinate of the pipe initiation location (m)
y	position in the y-direction (m)
y_i	y-coordinate of the pipe initiation location (m)
z	position perpendicular to the analysis plane (m)
Ω^S	soil subdomain
Ω^P	erosion pipe subdomain
μ	dynamic fluid viscosity (Ns/m^2)
τ	applied hydraulic boundary shear stress (Pa)
τ_c	critical boundary shear stress for incipient motion of sand grains (Pa)
θ	spatial correlation length (m)
ρ	correlation coefficient
ρ_w	fluid density (kg/m^3)

tip; (4) grains detach from the pipe tip; (5) laminar flow through the pipe channels that develops; and (6) the eroded sand grains are transported through the erosion pipe to the downstream exit. All of these processes must occur for BEP to progress to failure.

In addition to the experimental studies that provided an understanding of the BEP process, numerous studies have attempted to develop theoretical or numerical tools for predicting the progression of BEP (e.g., Sellmeijer, 1988, 2006; Schmertmann, 2000; Sellmeijer et al., 2011; Schweckendiek, 2014; Van Esch et al., 2013; Hoffmans and Van Rijn, 2018; Robbins, 2016; Robbins and Griffiths, 2018, 2021; Rotunno et al., 2019; Fascetti and Oskay, 2019). Some of these studies have attempted to predict pipe progression on the basis of the flow in the pipe (Sellmeijer, 1988; 2006; 2011;; Van Esch et al., 2013; Hoffmans and Van Rijn, 2018), while the rest have used the hydraulic conditions near the pipe tip as the basis for assessing pipe progression. Despite the numerous approaches, no universally accepted method for assessing pipe progression exists today. This can partially be explained by the fact that the methods are still incomplete, not yet accounting for all of the factors known to influence BEP progression (Robbins and Van Beek 2015, Van Beek, 2015). One such factor that has been shown to greatly impact BEP progression is that of soil variability (Negrinelli et al., 2016; Methorst, 2020). Through laboratory experiments on both uniform and layered soil deposits, Negrinelli et al. demonstrated that layered soils require up to 3 times more head differential to fail by BEP than uniform soils. This factor is not easily accounted for in the analysis of BEP, and the error of neglecting it is sufficiently large to limit the value of numerical methods that do not provide a means to account for soil variability. While some attempts at accounting for soil variability in BEP analysis have been

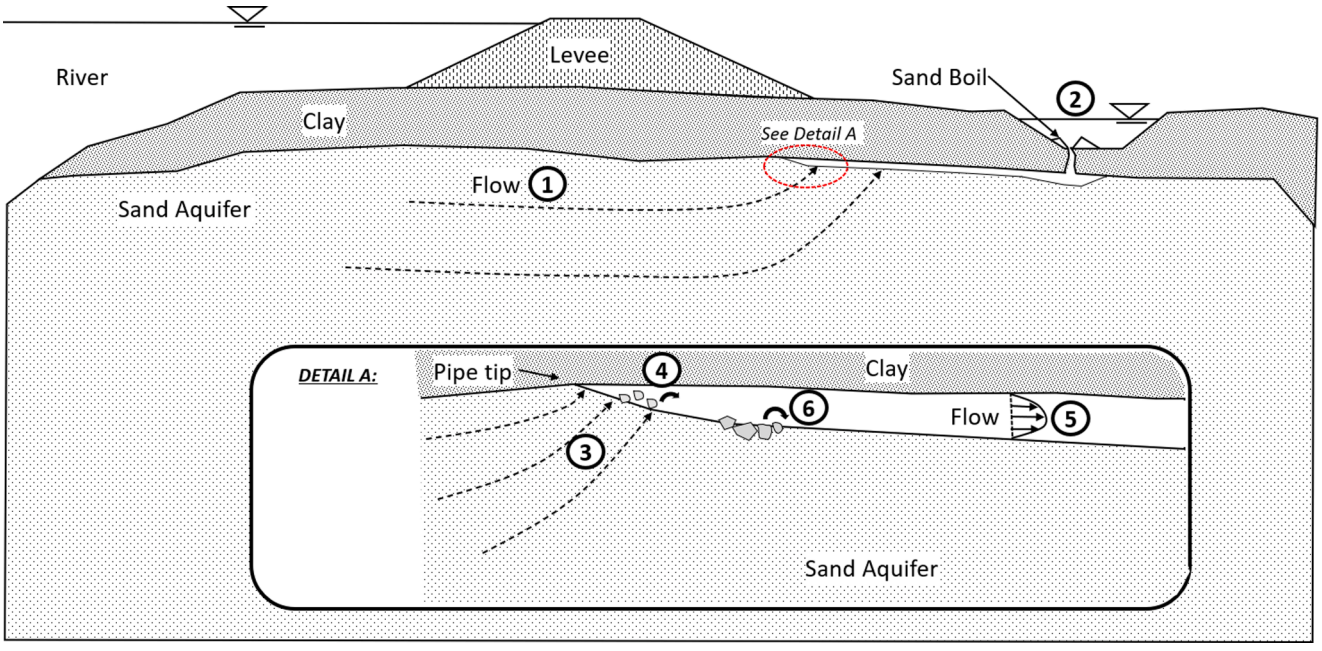

Fig. 1. Illustration of the backward erosion piping process (Robbins and Van Beek 2015).

made, these studies have either not explicitly simulated erosion (Liu et al. 2017), have simplified the erosion process (Kanning and Calle 2013), or have focused on other types of erosion (suffusion) that do not develop sequentially in the upstream direction (Liang et al. 2017).

This paper presents an application of the Random Finite Element Method (RFEM), developed by Griffiths and Fenton (1993) and Fenton and Griffiths (1993), to the simulation of BEP in order to quantitatively assess how spatial variability in soil properties influences pipe progression. The results presented herein greatly expand the initial presentation of results presented in Robbins et al. (2019) by assessing variability in both soil permeability and critical gradient for pipe progression.

2. RFEM simulation framework

RFEM is a combination of random field generation and finite element computations within a Monte-Carlo framework that is used to observe the influence of spatial variability in model properties on the statistics of model outputs. The results from RFEM analysis are useful for determining the sensitivity of model results to both the magnitude and patterns of spatial changes in model input properties, which in turn provides an indication of the overall structural reliability for various conditions. In the following sections, the finite element model used for simulating BEP is first discussed, followed by an overview of the random field generation and Monte-Carlo simulations used to perform RFEM analysis of BEP progression.

2.1. Two-dimensional finite element simulation of BEP progression

Various approaches have been taken in the literature for finite element modeling of backward erosion piping. As noted by Wang et al. (2014), continuum based BEP models can be separated into categories based upon how the eroded particles are tracked. The simplest approach is to model solely the influence of the erosion pipe on the groundwater flow while neglecting the sediment transport rate (Sellmeijer, 2006; Van Esch et al., 2013; Robbins and Griffiths, 2018). Alternatively, multiphase finite element formulations can be constructed that explicitly account for the eroded particles through inclusion of a fluidized soil phase that represents the eroded soil as it transits from the soil matrix to an eroded state in the pore fluid (Fujisawa et al., 2010; Rotunno et al., 2019). For this study, a piecewise-steady state approach was used to assess pipe progression, and the first category of modelling was followed in which only the hydraulic impacts of the erosion pipe on the groundwater flow are considered.

A finite element program called *rbep2d* was developed for assessing the progression of BEP through two-dimensional domains as illustrated in Fig. 2. The program was developed as an adaptation of the program for analysis of steady-state groundwater flow by Smith and Griffiths (2004). While the program is capable of performing analysis of BEP in two-dimensions in both plan view and profile view, only the plan view formulation will be described and demonstrated in this study.

With reference to Fig. 2, the problem consists of assessing the progression of BEP through a square or rectangular domain. As the analysis is conducted in plan view, the pipe can progress in any direction in the analysis plane. For this study, the progression of a pipe through a fixed domain of interest with unidirectional mean flow was assessed. As such, with reference to Fig. 2, the boundaries at $y = 0$ and $y = \mathrm{W}$ are no flow boundaries. The upstream and downstream boundaries ($x = 0$ and $x = \mathrm{L}$, respectively) are constant head boundaries, and the downstream boundary is fixed to $h = 0$. The pipe is initiated along the downstream boundary, and the upstream boundary condition is incrementally raised. For each head drop, the progression of the erosion pipe is simulated until equilibrium is found. This process is repeated until the equilibrium cannot be achieved and the pipe breaches the domain. In this manner, the limiting extent of pipe progression under steady state conditions can be found as a function of the boundary conditions.

The analysis domain is separated into a soil domain and a pipe domain as illustrated in Fig. 2. The groundwater flow in the soil domain is described by Darcy's equation

$$\frac{\partial}{\partial x}\left(k_x\frac{\partial h}{\partial x}\right)+\frac{\partial}{\partial y}\left(k_y\frac{\partial h}{\partial y}\right)=0 \tag{1}$$

where $h = z + p/\rho g$ is the piezometric head in terms of the elevation (z) perpendicular to the analysis plane, pore pressure (p), fluid density (ρ), and gravitational acceleration (g), and k_x and k_y are the hydraulic conductivities of the soil in the x- and y-directions, respectively. As the analysis is a two-dimensional plan view, groundwater flow through a plane of material with unit thickness is being considered.

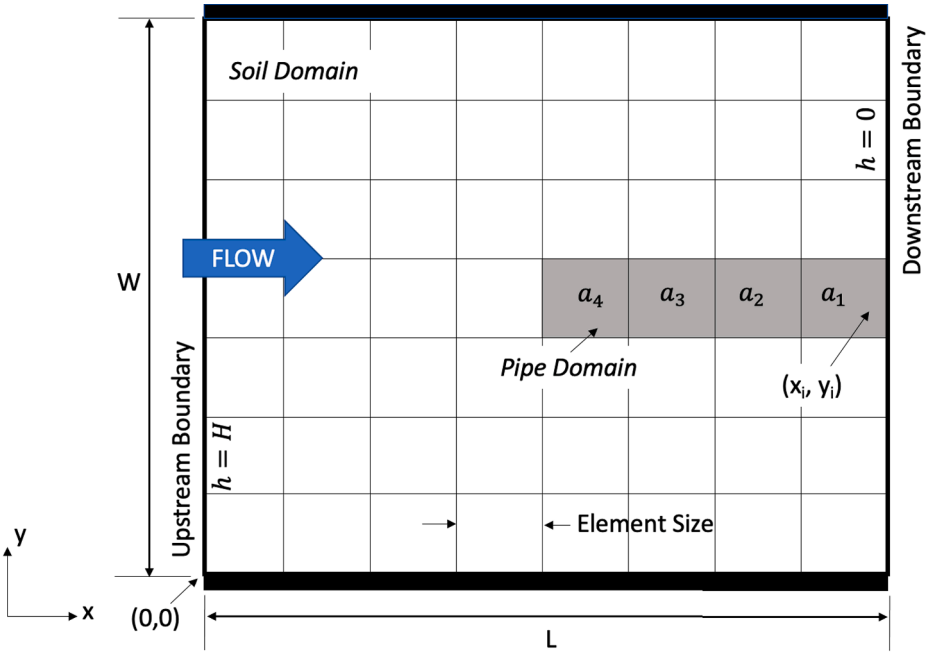

Fig. 2. Finite element mesh for two-dimensional, plan view, analysis of BEP progression.

The erosion pipe that forms is an open channel as illustrated by the photograph of a BEP pipe in Fig. 3. As such, the flow in the pipe is no longer considered flow through porous media. Instead, the flow in the pipe should be treated as pipe flow, which for steady-state conditions can be described by the Darcy–Weisbach equation

$$\frac{dh}{dx} = \frac{V^2}{2g}\frac{f}{D_H} \tag{2}$$

where V is the average flow velocity, $D_H = 4A/P$ is the hydraulic diameter for a pipe with area A and wetted perimeter P, and f is the friction factor.

The friction factor f accounts for the change in resistance due to flow regime (laminar vs. turbulent), and the hydraulic diameter D_H accounts for the differences in resistance caused by pipe cross sectional shape. While some authors have assumed the pipe cross section is circular (Rotunno et al. 2019), experimental studies have found that pipe cross sections typically have aspect ratios of $w/a = 10$ to 50 where a denotes the pipe depth and w denotes the pipe width (e.g. Hanses, 1985; Van Beek, 2015; Vandenboer, 2019). Similar aspect ratios were observed by Hanses for the pipe in Fig. 3. For these conditions, it is reasonable to follow the approach taken by Sellmeijer (1988); (2006;); Van Esch et al. (2013) where the flow in the pipe is considered to be laminar flow between two parallel plates. For this condition, Equation 3 takes the form of Darcy's law

$$V = \frac{a^3\rho_w g}{12\mu}\frac{dh}{dx} = k_{pL}\frac{dh}{dx} \tag{3}$$

where

$$k_{pL} = \frac{a^3\rho_w g}{12\mu} \tag{4}$$

is the equivalent hydraulic conductivity for laminar pipe flow in a pipe of depth a. As such, the steady state solution for flow in a pipe of depth $a = f(x,y)$ can be determined by letting $k_x = k_y = k_{pL}$ in Equation (1). In this manner, the solution for the coupled pipe flow and groundwater flow is completely described by Equations 1 and 4. This analogue between laminar flow between parallel plates and groundwater flow has long been recognized and formed the basis for viscous flow groundwater models (Harr, 1962). More details regarding Equation 4 as well as formulations for turbulent flow conditions are presented in Robbins and Griffiths (2021).

Using the Galerkin weighted residual method, the finite element discretization of Equation (1) is given by (e.g. Smith and Griffiths 2004)

$$[K_e]\{H\} = \{Q\} \tag{5}$$

Fig. 3. Photograph of a BEP erosion channel for test number 23 (Hanses, 1985).

where $\{H\}$ and $\{Q\}$ denote the total head and net flow at the finite element nodes and

$$[K_e] = \sum_{\Omega^s}\int_{\Omega_e^s}\left(k_x\frac{\partial N_i}{\partial x}\frac{\partial N_j}{\partial x} + k_y\frac{\partial N_i}{\partial y}\frac{\partial N_j}{\partial y}\right)d\Omega_e^s + \sum_{\Omega^p}\int_{\Omega_e^p}k_{pL}\left(\frac{\partial N_i}{\partial x}\frac{\partial N_j}{\partial x} + \frac{\partial N_i}{\partial y}\frac{\partial N_j}{\partial y}\right)d\Omega_e^p \tag{6}$$

with Ω^s and Ω^P denoting the soil and pipe domains, respectively, and the subscript e denoting the element subdomains. Allowing the depth of the erosion pipe to vary as a_i for pipe elements $i = 1,\cdots,n$, Equation 4 can be applied to compute $[k_e]$ for each pipe element. The depth of the erosion pipe a_i is unknown; therefore, an iterative solution procedure is required. The pipe depth is determined based upon the equilibrium conditions of the sand on the bottom of the fictitious erosion pipe being represented by the pipe elements. For sand, there is a critical hydraulic shear stress τ_c at which grain transport begins (Shields, 1936; White, 1940). Treating the pipe as laminar flow between parallel plates separated by depth a, the magnitude of the hydraulic shear stress exerted on the boundaries of the erosion pipe is given for each pipe element by

$$\tau_i = \frac{a_i\rho_w g}{2}\left(\frac{dh^2}{dx} + \frac{dh^2}{dy}\right)^{1/2}. \tag{7}$$

The erosion pipe will deepen until the hydraulic shear stress magnitude is less than the critical hydraulic shear stress and Equation 8 is satisfied.

$$\tau < \tau_c \tag{8}$$

An overview of the algorithm for analysis of BEP progression is given in Fig. 4. Erosion is initiated at a location along the downstream boundary of the analysis domain by switching a soil element to a pipe element. The depth of the erosion channel in the pipe element is initialized to $a = 3d_{50}$ where d_{50} denotes the median grain size of the sand being eroded. The coupled groundwater and pipe flow equations are solved for the initial pipe depth using Eqs. (4)–(6). Once a solution has been obtained, τ is calculated and Equation 8 is evaluated. If $\tau < \tau_c$ the pipe will not deepen further, and the solution has been obtained. If Equation 8 is not satisfied, the pipe depth in elements for which Equation 8 is violated is increased by $d_{50}/2$ and the problem is solved again. This process is repeated until the appropriate pipe depth for satisfying Equation 8 has been determined in all pipe elements.

Once the pipe depth has been determined and a hydraulic solution for the coupled flow problem has been obtained, the progression of the erosion pipe can be assessed. For this study, the pipe progression was assessed on the basis of the hydraulic gradients in the neighboring soil elements (elements sharing nodes with pipe elements). For all neighboring soil elements, the magnitude of the hydraulic gradient given by Equation 9 was compared to a user defined critical, hydraulic gradient for pipe progression (i_{cr}). If $i_h > i_{cr}$ in any adjacent soil elements, the element with the greatest value of $(i_h - i_{cr})$ was switched to a pipe element, the pipe depth in that element was set to the initial pipe depth of $a = 3d_{50}$, and the iterative procedure for solving for the pipe depth was repeated. This process is continued until $i_h < i_{cr}$ in all soil elements adjacent to the erosion pipe.

$$i_h = |\nabla h| = |[\nabla N_i]\{H\}| \tag{9}$$

Once equilibrium has been reached under a given set of boundary conditions, the upstream boundary condition is increased if the pipe has not passed completely through the domain or a maximum desired value for the upstream boundary condition has not yet been reached. For this study, the upstream boundary condition was increased in increments of 1 percent of the assigned value. Once the total head on the upstream boundary has been increased, the iterations on pipe depth are conducted again, followed by the evaluation of pipe progression. In this manner, the progression of the pipe through the domain can be assessed to

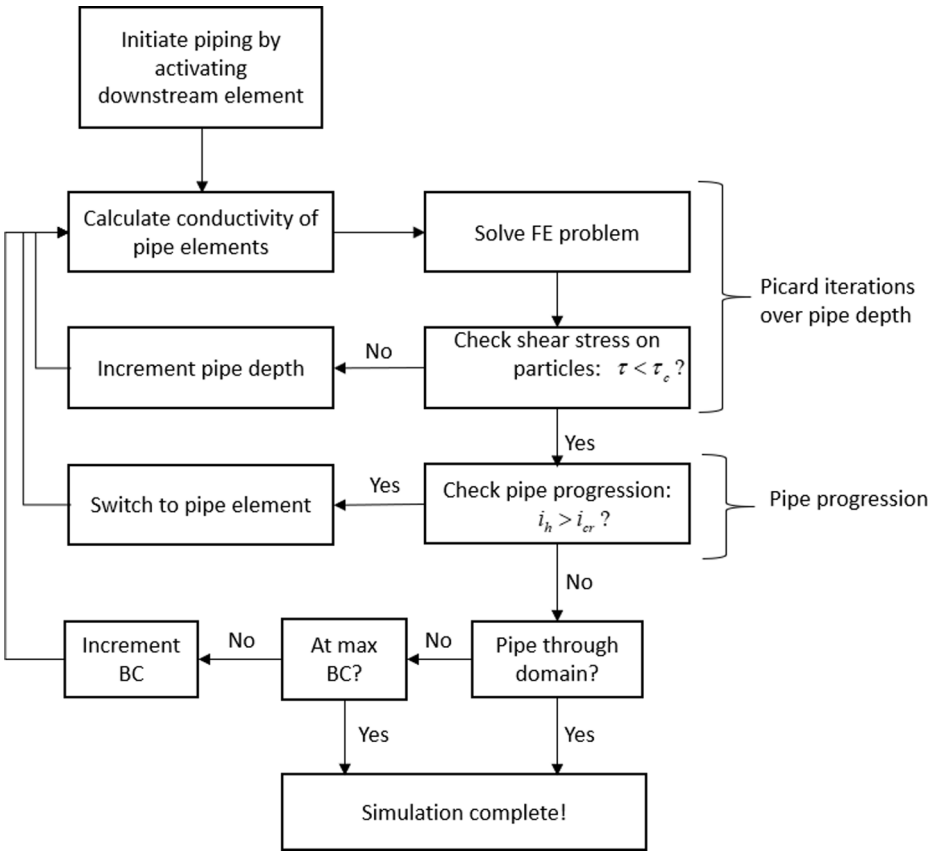

Fig. 4. Algorithm for finite element analysis of BEP progression.

determine the degree of pipe progression for each applied boundary condition as shown in Fig. 5 where H/L denotes the average hydraulic gradient across the domain. The value of H/L at which the erosion pipe progresses completely through to failure is called the critical, average hydraulic gradient. While Fig. 5 illustrates an example pipe progression curve for a single analysis, RFEM permits the influence of random soil properties on the resulting distribution of $(H/L)_{cr}$ to be assessed probabilistically.

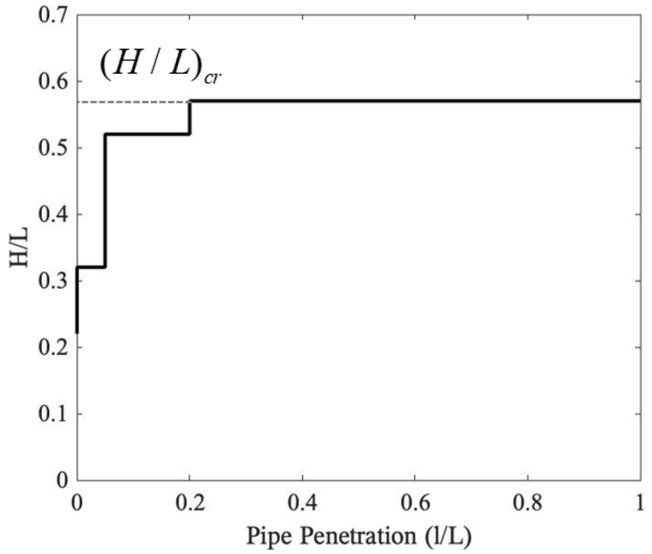

Fig. 5. Example pipe progression curve.

2.2. Random field generation

The soil properties with the greatest influence on the pipe progression are the hydraulic conductivity of the soil and the critical hydraulic gradient for pipe progression (Schmertmann, 2000; Sellmeijer et al., 2011). The hydraulic conductivity of the soil determines the magnitude of flow towards the pipe, and thus the pipe dimensions. The spatial variation of the hydraulic conductivity also dictates the spatial distribution of hydraulic gradient in the soil. Both of these factors control the magnitude of the hydraulic gradients near the progressing pipe tip. Meanwhile, the resistance to pipe progression is dictated by the critical hydraulic gradient for pipe progression. Therefore, the soil hydraulic conductivity and critical hydraulic gradient were both treated as the random fields for the RFEM analyses.

As both the hydraulic conductivity k and critical hydraulic gradient i_{cr} are related to the grain size distribution of the soil (e.g., Carrier, 2003; Schmertmann, 2000), it is necessary to allow the k-field and i_{cr}-field to be cross-correlated. For uniformly graded soils, both k and i_{cr} increase with increasing grain size and the fields are positively correlated. For well graded soils, k can decrease as the fine fraction of the soil decreases in grain size which causes i_{cr} to increase in magnitude due to increasing uniformity coefficient of the soil (Schmertmann 2000). In this scenario, the random fields will be negatively correlated. As such, both positive and negative correlations were considered herein.

For this study, both k and i_{cr} were treated as lognormally distributed random variables. To generate the cross-correlated random fields for each variable, the covariance matrix decomposition method was used (Fenton, 1994; Fenton and Griffiths, 2008). Two independent Gaussian random fields were generated using the Local Average Subdivision (LAS) method (Fenton and Vanmarcke 1990) with specified correlation length $\theta = \theta_x = \theta_y$ and a Markov correlation function (Fenton and Griffiths 2008). The covariance decomposition method was then used to generate

a third Gaussian field that had a specified correlation to the first field. The two correlated random fields were then transformed to the desired marginal distributions for each of the two variables of interest.

2.3. Monte-Carlo Simulation

In RFEM analysis, it is necessary to perform Monte-Carlo simulations to generate meaningful and accurate statistics of output quantities of interest. For analysis of BEP, the critical average hydraulic gradient $(H/L)_{cr}$ is the quantity of interest. From the distribution of this quantity, the probability of BEP pipe progression through the analysis domain can be evaluated under various conditions.

The Monte-Carlo simulation loop follows the steps outlined in Fig. 6. For each Monte-Carlo simulation, a new realization of the i_{cr} and k random fields is generated according to the specified random field parameters. The FEM analysis of the pipe progression is performed following the approach described in Section 2.1, resulting in a single pipe progression curve as illustrated in Fig. 5. The value of $(H/L)_{cr}$ for each simulation is determined by post processing the results to find the maximum value of (H/L) reached during the analysis. The $(H/L)_{cr}$ value from the simulation is stored, and this process is repeated for subsequent simulations until the distribution of $(H/L)_{cr}$ for the particular RFEM analysis has been adequately defined.

3. Example problem

A simple example problem was developed to illustrate the RFEM approach described in this study for a 10-m by 10-m domain as illustrated in Fig. 7. The boundaries at $y = 0$ and 10 m are no flow boundaries. The boundary at $x = 10$ m is a constant head boundary with $h = 0$ m. The boundary at $x = 0$ m is the constant head, upstream boundary. An initial condition of $h = 0.1$ m was assigned to the upstream boundary, and head was increased each time the pipe reached equilibrium until the pipe progressed through the domain. For nearly all analyses conducted, the pipe was initiated at the center of the downstream boundary. For a few analyses, the pipe was allowed to initiate anywhere along the boundary to assess the influence of an unrestricted initiation location on the results.

An element size of 0.125 m was used such that the domain was a square with 80 elements in both the x- and y- directions for a total of 6400 elements. All elements were 4 node quadrilateral elements with linear shape functions.

Assumed soil properties, water properties, and random field characteristics for the example problem are listed in Table 1. The mean values of soil properties were selected to represent a fine-grained sand with a median grain size of $d_{50} = 0.2$ mm. The mean hydraulic conductivity for a sand of this particle diameter is approximately $\mu_k = 1.0 \times 10^{-5}$ m/s (Van Beek 2015), and the critical shear stress has been shown to be $\tau_c = 0.33$ Pa (Van Beek et al. 2019). The mean value of the critical hydraulic gradient for pipe progression for fine sand is approximately $\mu_{icr} = 0.3$ (Robbins et al. 2018) when assessed over the distance of 1 element (0.125 m). In addition, values of $\mu_{icr} = 1.0$ and 3.0 were also considered to assess the influence of the critical hydraulic gradient magnitude on the results. The density (ρ_w) and dynamic viscosity (μ) of water were selected assuming a water temperature of 20 degrees Celsius.

While the mean properties for fine sand are well defined, less information on the spatial variability of these properties in the field is available, which may also be site specific. As such, a broad range of random field characteristics was assumed for this study to evaluate the general trends caused by random soil properties. All analyses considered were for isotropic random fields in which $\theta_x = \theta_y = \theta$. Five values of θ/L were considered in this study ranging from 0.05 to 1.0. For the hydraulic conductivity random field, k was assumed to be lognormally distributed with a mean of $\mu_k = 1 \times 10^{-5}$ m/s with five values of coefficient of variation (σ_k/μ_k) ranging from 0.25 to 3.0. To initially investigate the influence of randomness in only the hydraulic conductivity k, a set of analyses were conducted with a uniform, deterministic value of $i_{cr} = 0.3$ ($\sigma_{icr} = 0.0$). Subsequently, various i_{cr} random fields were considered with means 0.3, 1.0, and 3.0 and coefficients of variation for the critical gradient (σ_{icr}/μ_{icr}) of 0.16, 0.5, and 1.0. When random fields were also generated for the critical gradient, i_{cr} was also assumed to be lognormally distributed with the same spatial correlation length as the k-field. Values of correlation between the two random fields evaluated were $\rho = -1$, 0, and 1. These input parameters resulted in 25 different k-fields and 9 different i_{cr}-fields that were evaluated. Each of these combinations was re-evaluated for the 3 different correlation values resulting in 675 different input variable combinations. Considering the additional 25 scenarios with $\sigma_{icr} = 0.0$, a total of 700 combinations of input parameters were evaluated, with a separate Monte-Carlo analysis being conducted for each scenario. A single, sample realization from one of the analysis scenarios is shown in Fig. 8. While the result of a single realization does not yield meaningful information regarding $(H/L)_{cr}$, it does provide a nice illustration of the BEP behavior in random fields. It is readily seen that the pipe is meandering through the domain, searching for the path of least resistance. Further, the influence of the pipe on the groundwater flow pattern can be seen from the flow net drawn in Fig. 8a. The erosion pipe is capturing nearly all flow in the domain, and the hydraulic gradient is high near the upstream pipe tip as indicated by the closely spaced head contours. While the results of every realization could not be examined, some of the trends that will best be explained in terms of some of these observed behaviors. The full distributions of results obtained from the RFEM analysis are presented and discussed in the next section.

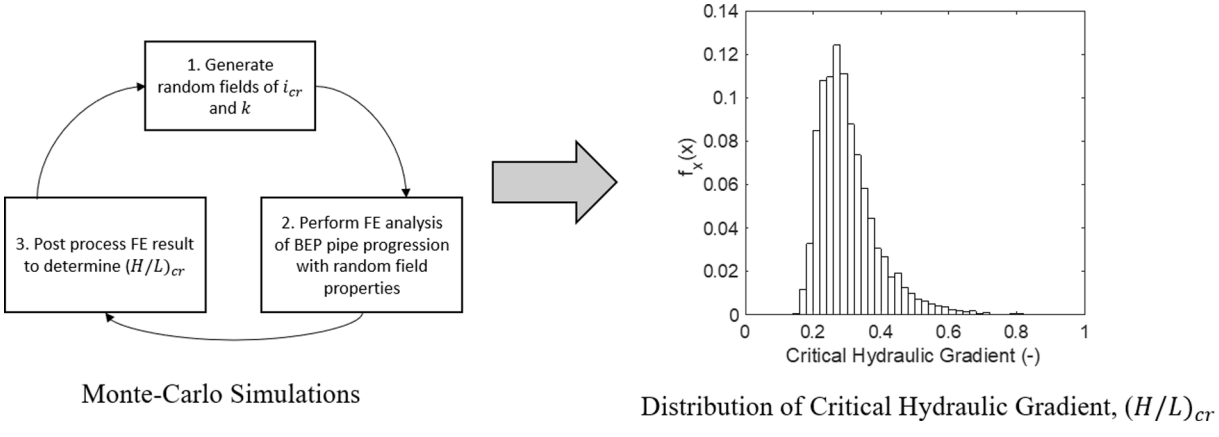

Fig. 6. Illustration of Monte-Carlo analysis loop for BEP RFEM analysis.

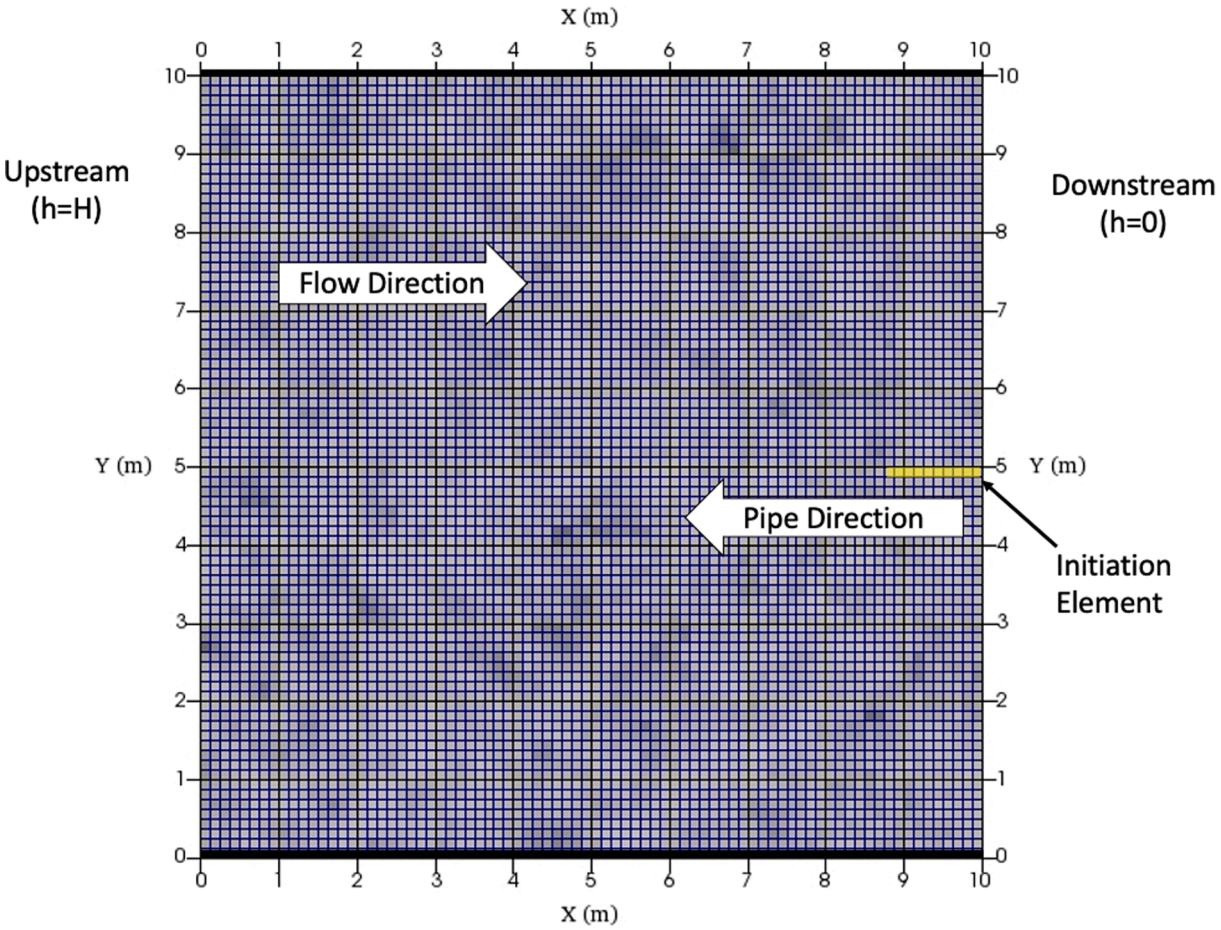

Fig. 7. Example problem for RFEM analysis.

Table 1
Model inputs values for example problem.

Property	Value
d_{50}(mm)	0.2
μ_k(m/s)	1.0×10^{-5}
τ_c(Pa)	0.33
μ_{icr}	0.3, 1.0, 3.0
ρ_w(kg/m^3)	1,000
μ(Ns/m^2)	0.001
σ_k/μ_k	0.25, 0.5, 1.0, 2.0, 3.0
σ_{icr}/μ_{icr}	0.0, 0.16, 0.5, 1.0
θ/L	0.25, 0.5, 1.0, 2.0, 3.0
ρ	−1.0, 0.0, 1.0

4. RFEM analysis results

The RFEM analyses were conducted on a Cray supercomputer using a program written in Fortran with OpenMPI. The supercomputer was used for this study due to the number of computations required. Each BEP finite element analysis consisted of 200–400 computational steps (for upstream head increments and pipe progression steps). The precise number of steps depended on the resistance of the soil to pipe progression, with more steps required for analyses requiring higher hydraulic gradients for progression of the pipe through the domain. At each step, the Picard iterations on the pipe depth also had to be performed such that Equation (1) was solved approximately 1000 times per BEP analysis. Considering the 700 combinations of input parameters, this study required that Equation (1) be solved approximately 700,000 times per Monte-Carlo simulation that was conducted. As such, it was desired to minimize the number of simulations conducted to reduce the computational time required as much as possible. A discussion on the computational performance of the program and RFEM convergence is briefly presented prior to discussing the quantitative RFEM results.

All Monte-Carlo analyses were conducted on a Cray supercomputer at the U.S. Army Engineering Research and Development Center Supercomputing Resource Center named Onyx. The Onyx HPC is a Cray XC40/50 with 4810 standard compute nodes. Each node has dual, 22-core Intel E5-2699v4 Broadwell processors with 2.8 GHz core speeds for a total of 44 cores per node. All of the analyses in this study were run on 10 nodes using 440 cores. An evaluation of the runtime was performed for the case with the highest coefficients of variation in both the k- and i_{cr}-fields. This case was used for timing as it was one of the longer simulations. As seen in Fig. 9, the run time varied linearly with the simulation count due to the "embarrassingly" parallel nature of the RFEM simulation process.

The convergence of the Monte-Carlo analysis was assessed by evaluating the mean and standard deviation of the critical gradient, $(H/L)_{cr}$, as the number of Monte-Carlo simulations increased. An example convergence plot for a case with high variance in the hydraulic conductivity random field is shown in Fig. 10. The case with $\sigma_k/\mu_k = 3.0$ was selected for assessing convergence as the scenarios with the most variability converged the slowest. Additionally, as illustrated in Fig. 10, the scenarios with the largest spatial correlation length (θ) converged the slowest. The analysis case with the smallest spatial correlation length converged rather quickly (<1000) simulations. While the convergence of the standard deviation for the case of $\theta/L = 1.0$ in Fig. 10b is not quite established by the time it reaches 4400 simulations, it may be close enough for the purposes of this study in which only general trends in the

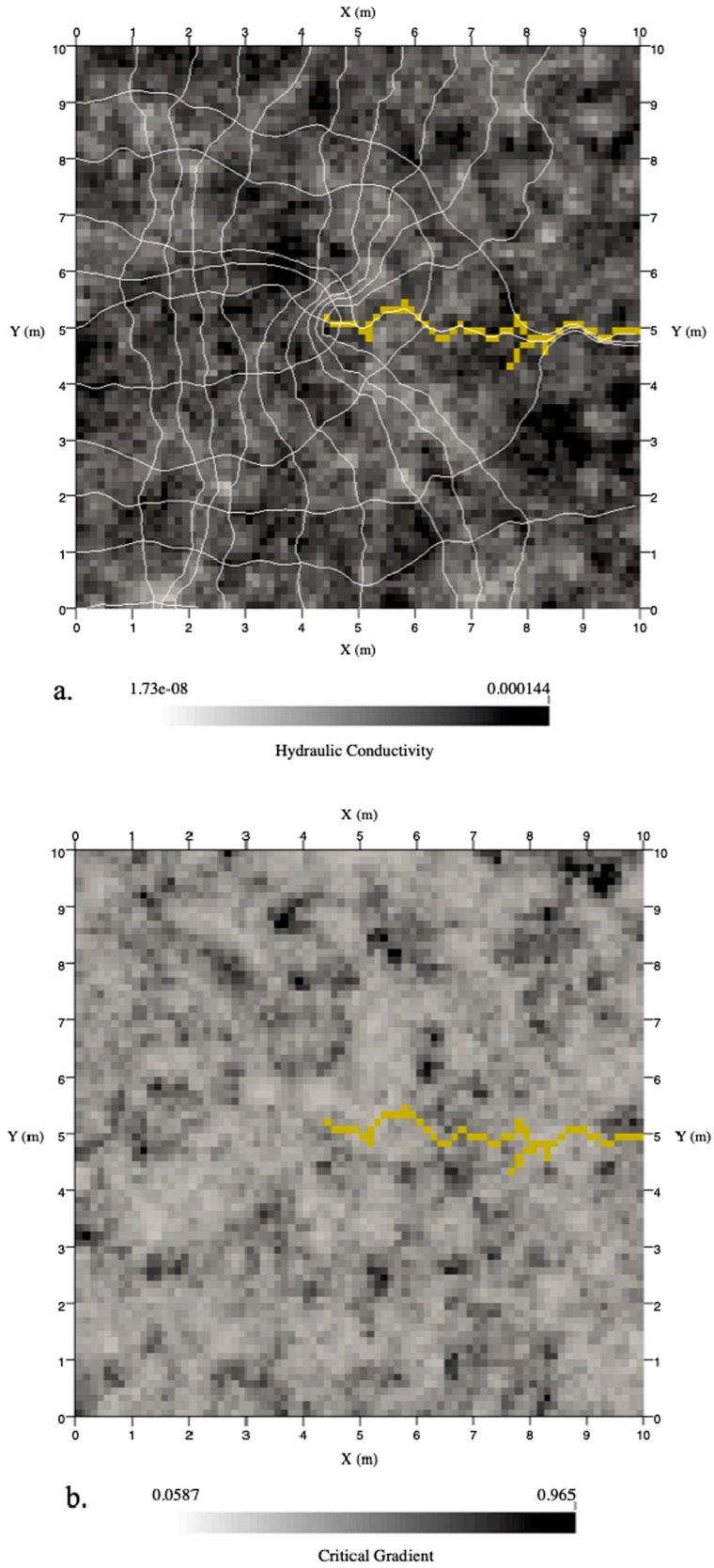

Fig. 8. Example realization showing (a) k-field with head contours and pipe path and (b) i_{cr}-field with pipe path for scenario with $\sigma_k/\mu_k = 3$, μ_{icr}=0.3, σ_{icr}/μ_{icr}=0.5, ρ=0, and $\theta = 0.5$ m.

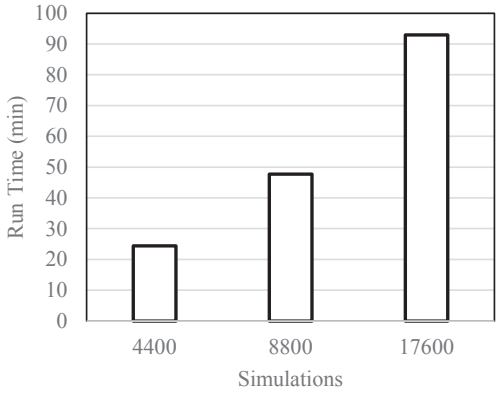

Fig. 9. Runtimes for MPI Monte-Carlo simulations on 440 cores.

critical gradient distributions are being assessed. The error in the estimated probability of failure (p_f) can be calculated with confidence level $(1-\alpha)$ as (Fenton and Griffiths, 2008)

$$e = \frac{z_{\alpha/2}}{\sqrt{\frac{n}{p_f(1-p_f)}}} \tag{10}$$

where $z_{\alpha/2}$ denotes the point on the normal distribution corresponding to $P[Z > z_{\alpha/2}] = \alpha/2$ and n is the number of Monte-Carlo simulations. For the case of n = 4400 and $p_f = 0.05$, e was estimated to be 0.005 with 90% confidence, or 10% error. This was deemed adequate for the purposes of the present study. As such, 4400 simulations were selected as the number of Monte-Carlo simulations for use in the analysis to keep computational times to reasonable levels. As the error will increase with lower values of p_f, a value of $p_f = 0.05$ was the lowest probability on the distribution evaluated in the present study. The results of all analysis are discussed in the sections that follow, first focusing on trends due to hydraulic conductivity variability alone, followed by sections that discuss the influence of i_{cr} spatial variability and the erosion initiation location.

4.1. Random k-field results

The 25 scenarios with hydraulic conductivity as the only random variable were run initially. To visualize the results, the empirical cumulative distribution function (CDF) of the $(H/L)_{cr}$ values obtained from the Monte-Carlo analysis was generated for each case. The five CDFs for the smallest and largest correlation lengths are illustrated in Fig. 11a and 11b, respectively. The probability on the y-axis represents the percentage of Monte Carlo simulations that progressed to failure at or below the associated gradient value. This can be interpreted as the probability of failure.

From Fig. 11, it is readily seen that increasing the coefficient of variation of the hydraulic conductivity random field causes the CDF to shift to the right. For low correlation lengths (Fig. 11a), the entire CDF shifts to the right at all probability values. This indicates that any increase in variability leads to increasing resistance against piping if the correlation length is small relative to the analysis domain. For large correlation lengths (Fig. 11b), increasing variability causes the low probability range of the CDF to shift to the left, meaning pipe progression becomes more likely. However, for large probability values, the distribution still tends to shift towards the right. The low probability value range (<10%) of the CDF is often of great interest for risk assessments as target failure probabilities are typically low. Therefore, to capture the trend observed for low probabilities, the value of the critical, average hydraulic gradient associated with $p_f = 5\%$ was extracted from the CDFs for all 25 cases. Fig. 12 illustrates the resulting trends in the critical, average hydraulic gradients associated with $p_f = 5\%$ as a function of both θ and σ_k/μ_k. From these results, it is seen that for $\theta/L = 0.05$, 0.10, and 0.25, increasing σ_k/μ_k leads to an increase in the gradient associated with $p_f = 5\%$ indicating that piping is less likely with increasing variance. For the larger correlation lengths, increasing σ_k/μ_k leads to smaller hydraulic gradients indicating that piping is more likely. Lastly, regardless of the value of σ_k/μ_k, the hydraulic gradient required to cause failure decreases with increasing correlation length. The extent of this trend will be evaluated more thoroughly when discussing the results with random i_{cr} and random k-fields.

4.2. Combined k-field and i_{cr} field results

Each of the 25 scenarios with random hydraulic conductivity were repeated an additional 27 times to assess the combined influence of both spatially variable k and i_{cr}. The resulting CDFs of all 675 Monte-Carlo simulations were assessed graphically to evaluate trends. Two trends were observed universally in all of the results, as illustrated by the select CDFs for the extreme correlation lengths and hydraulic conductivity coefficients of variation shown in Fig. 13. In all cases, as the coefficient of variation of i_{cr} increases, the CDF shifts to the left indicating that BEP progression is increasingly likely. This trend was exhibited in all of the scenarios. As might be expected, the second trend observed was that any

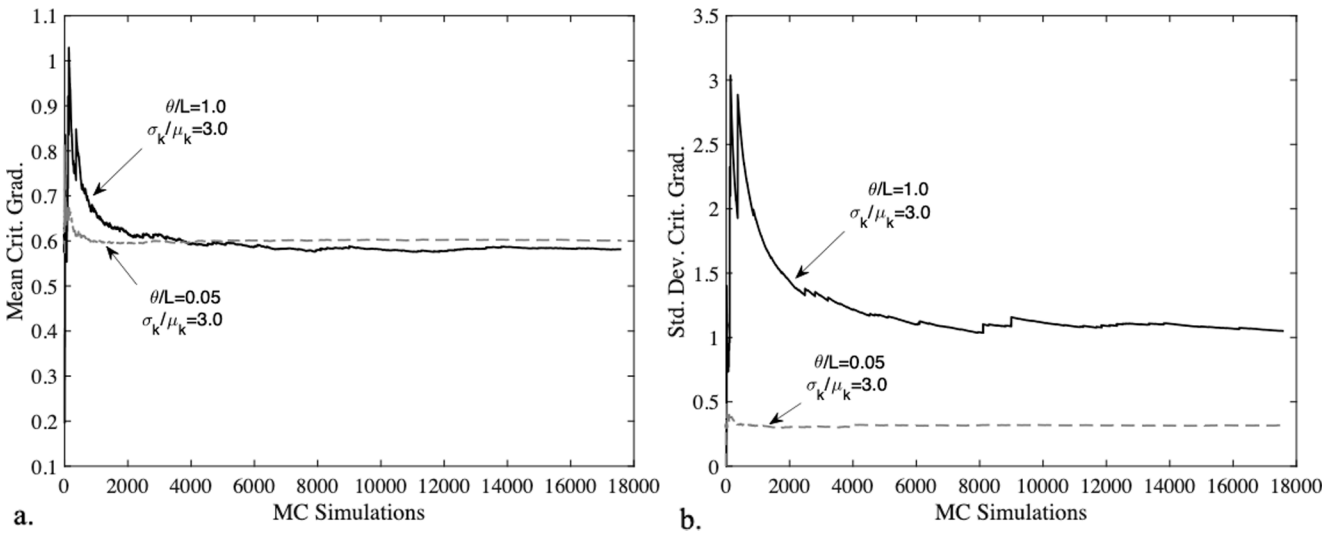

Fig. 10. Convergence of the (a) mean and (b) standard deviation of the critical, average hydraulic gradient for case with $\mu_{icr} = 0.3$, σ_{icr}=0.3, and $\rho = 0$.

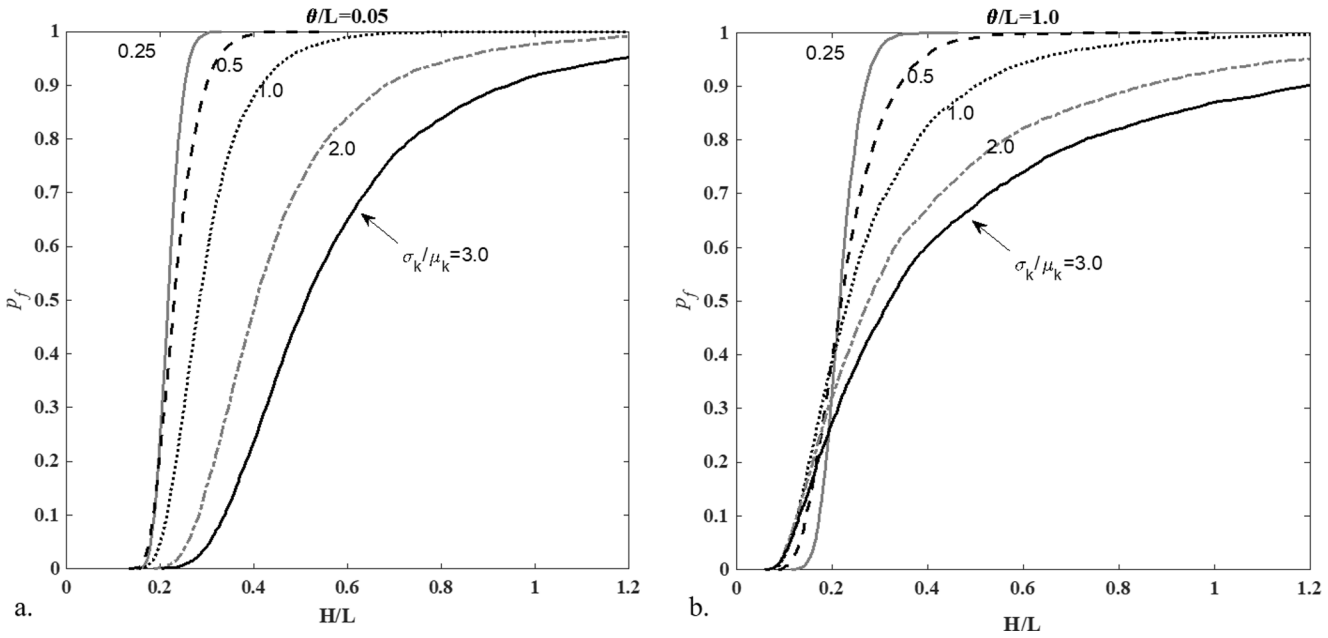

Fig. 11. Cumulative distribution functions for $i_{cr} = 0.3$with k as the only random variable for (a) smallest correlation length and (b) largest correlation length.

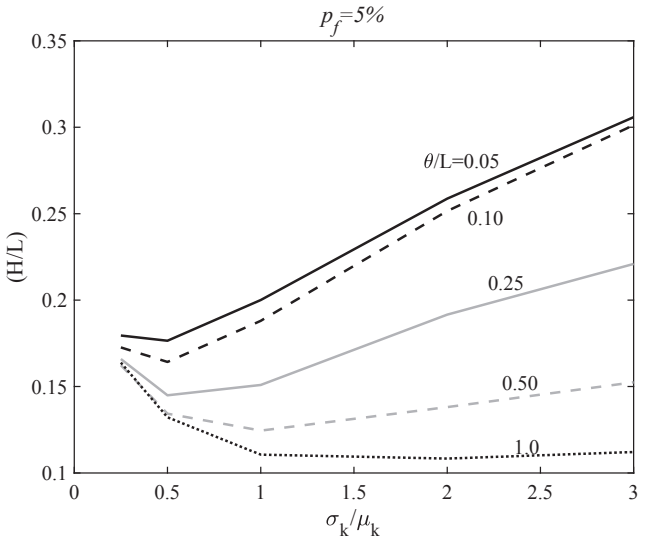

Fig. 12. Influence of k coefficient of variation and θ on gradient associated with p(f) = 5%.

increase in μ_{icr} leads to a direct increase in the hydraulic gradient required for pipe progression. This is readily seen in Fig. 13 by comparing the CDFs for $\mu_{icr} = 0.3$ and $\mu_{icr} = 1.0$.

In addition to understanding the influence of i_{cr} on the results, it was also of interest to see if the gradient required to cause BEP failure still decreased with increasing correlation length. To assess this trend more thoroughly, a few additional analyses were also run for cases with larger values of θ. The trend in the hydraulic gradients associated with the 5%, 25%, 50%, 75%, and 95% failure probabilities for one particular case is illustrated in Fig. 14. Just as before, the hydraulic gradient for $p_f = 5\%$ decreases continually with increasing values of θ. This observation clearly highlights that large correlation lengths are the worst-case scenario when dealing with the low probability of failure range of the CDFs. Interestingly, for higher values of p_f, the highest value of hydraulic gradient required to achieve the given p_f value is associated with $0.5 < \theta/L < 1.0$.

The influence of the correlation between the hydraulic conductivity field and the critical gradient field was also of interest. After evaluating the influence of ρ for all 675 scenarios, it was determined that two different trends were seen in the results as illustrated in Fig. 15. For low values of σ_k and σ_{icr}, changing the value of ρ caused the distributions to cross over each other as indicated in Fig. 15a. In this instance, $\rho = -1$ decreased the probability of BEP progression in the low probability arrange, and $\rho = 1$ only slightly increased the probability of BEP progression in the low probability range. Once the value of σ_k/μ_k was equal to or greater than 0.5 or the value of σ_{icr}/μ_{icr} was greater than 0.16 (see Table 1), the influence of ρ changed to that indicated in Fig. 15b. In these cases, ρ simply shifted the CDF to the left or right, depending on the value of ρ. Values of $\rho = -1$ shifted the CDF to the left indicating that BEP was more likely, whereas values of $\rho = 1$ shifted the CDF to the right indicating BEP progression was less likely.

While the influence of ρ on the failure probabilities was clearly defined using the extreme values of $\rho = -1$ and 1, it is of interest to try and determine a realistic value for ρ to be able to make conclusions regarding the expected influence of ρ. To the authors knowledge, the correlation between k and i_{cr} has never been evaluated in the literature. To make a realistic estimate of the value of ρ, the laboratory data presented in Robbins et al. (2021) was evaluated. This study measure both the k and i_{cr} in cylindrical, laboratory flume tests for uniformly graded sands of various sizes. A plot of the measured k and i_{cr} values is illustrated in Fig. 16. The correlation coefficient was found to have a value of $\rho = 0.7$ for this data set. It should be emphasized that this value of ρ only applies to clean, uniformly graded sands. For poorly graded soils, it is expected that the correlation may in fact be negative in value as an increasing fine fraction leads to low permeabilities and high Cu values, which have been shown to be quite resistant to piping (Schmertmann 2000).

As uniformly graded soils tend to have lower values of i_{cr} and less spatial variability, the CDF shown in Fig. 15a may be considered relatively typical for these types of soils. As shown, the value of $\rho = 0.7$ has little influence on the resulting CDF. For uniform soils, it is thus seen that the value of ρ is not very significant, and a value of 0.7 can be used as a reasonable estimate for uniform soils without causing significant error.

The previous presentation illustrated the general trends observed in the results obtained with both random k- and i_{cr}-fields; however, it was not possible to present the quantitative results obtained for all of the

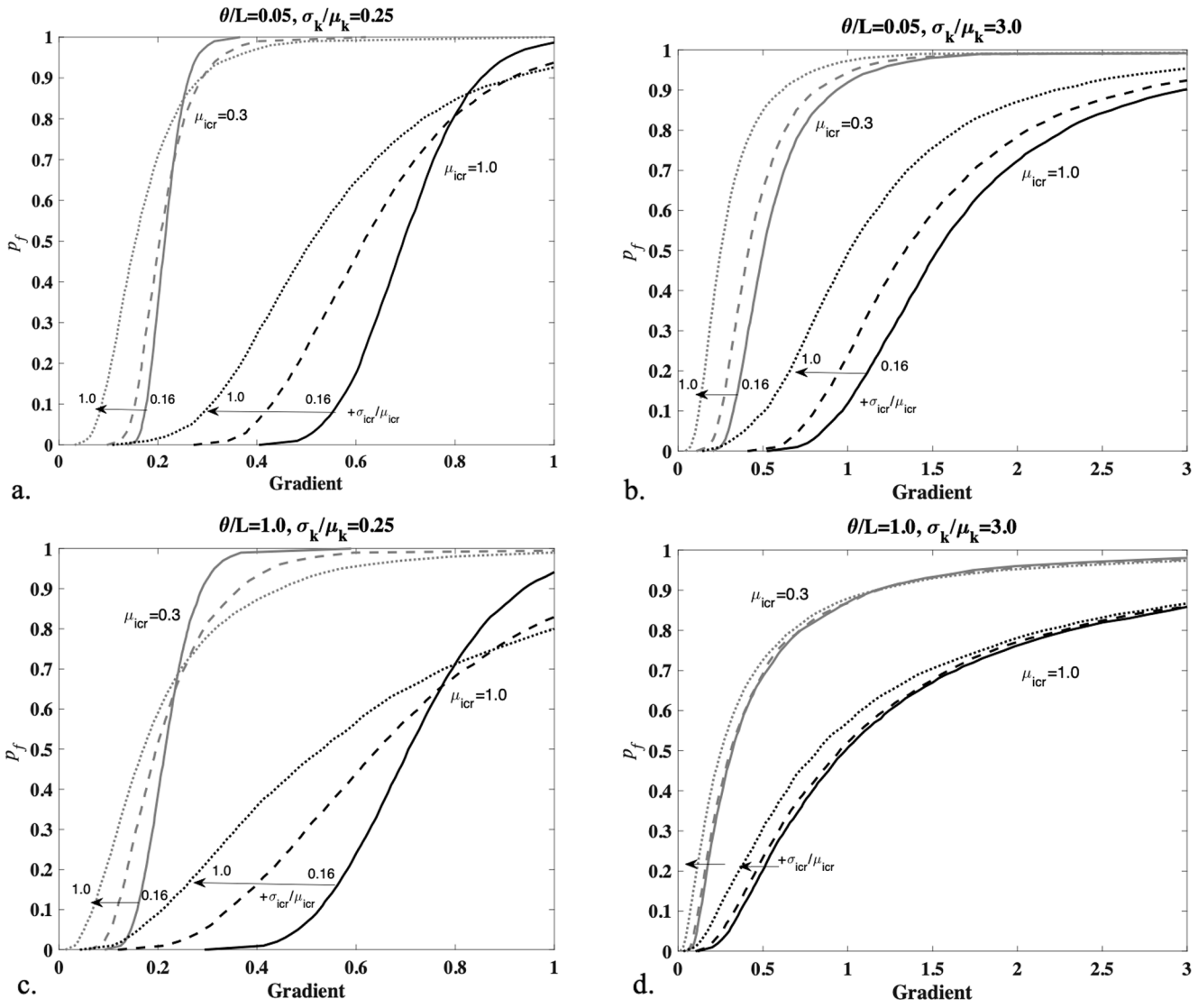

Fig. 13. Influence of i_{cr} random field on probability of failure.

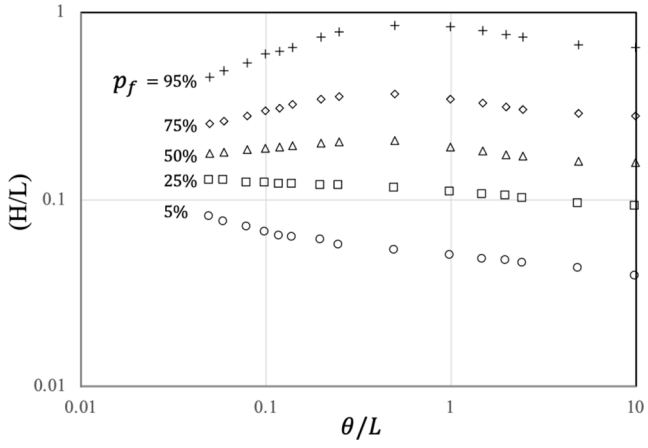

Fig. 14. Influence of correlation length on failure probabilities for $\sigma_k/\mu_k = 1$, μ_{icr}=0.3, σ_{icr}=0.3, and $\rho = 1$.

analysis conducted. To share the complete set of RFEM results with the interested reader, the resulting $(H/L)_{cr}$ distributions computed for each scenario were fitted to lognormal distributions (Fig. 17). The mean ($\mu_{\ln((H/L)_{cr})}$) and standard deviation ($\sigma_{\ln((H/L)_{cr})}$) of the natural logarithm of $(H/L)_{cr}$ for the best fit distribution was determined for each scenario. A regression analysis was then performed to try and develop a reduced order model that predicted the resulting mean and standard deviation of ln $(H/L)_{cr}$ as a function of the input variables σ_k/μ_k, θ/L, σ_{icr}/μ_{icr}, μ_{icr}, and ρ. The resulting equations developed for predicting $\mu_{\ln((H/L)_{cr})}$ and $\sigma_{\ln((H/L)_{cr})}$ are presented as Equations 10 and 11, respectively. The coefficient of determination was equal to 0.98 for Equation 10 and 0.88 for Equation 11.

$$\mu_{\ln((H/L)_{cr})} = -2.2001 + 0.337\frac{\sigma_k}{\mu_k} + 0.250\frac{\theta}{L} + 2.223\mu_{icr} - 0.084\frac{\sigma_{icr}}{\mu_{icr}} + 0.162\rho - 0.018\left(\frac{\sigma_k}{\mu_k}\right)^2 - 0.361\left(\frac{\theta}{L}\right)^2 - 0.421\mu_{icr}^2 - 0.264\left(\frac{\sigma_{icr}}{\mu_{icr}}\right)^2 - 0.017\rho^2 \quad (10)$$

$$\sigma_{\ln((H/L)_{cr})} = -0.018 + 0.235\frac{\sigma_k}{\mu_k} + 1.007\frac{\theta}{L} + 0.012\mu_{icr} + 0.185\frac{\sigma_{icr}}{\mu_{icr}} + 0.105\rho - 0.030\left(\frac{\sigma_k}{\mu_k}\right)^2 - 0.680\left(\frac{\theta}{L}\right)^2 - 0.003\mu_{icr}^2 + 0.133\left(\frac{\sigma_{icr}}{\mu_{icr}}\right)^2 - 0.012\rho^2 \quad (11)$$

Equation 10 and 11 can then be used to predict the lognormal

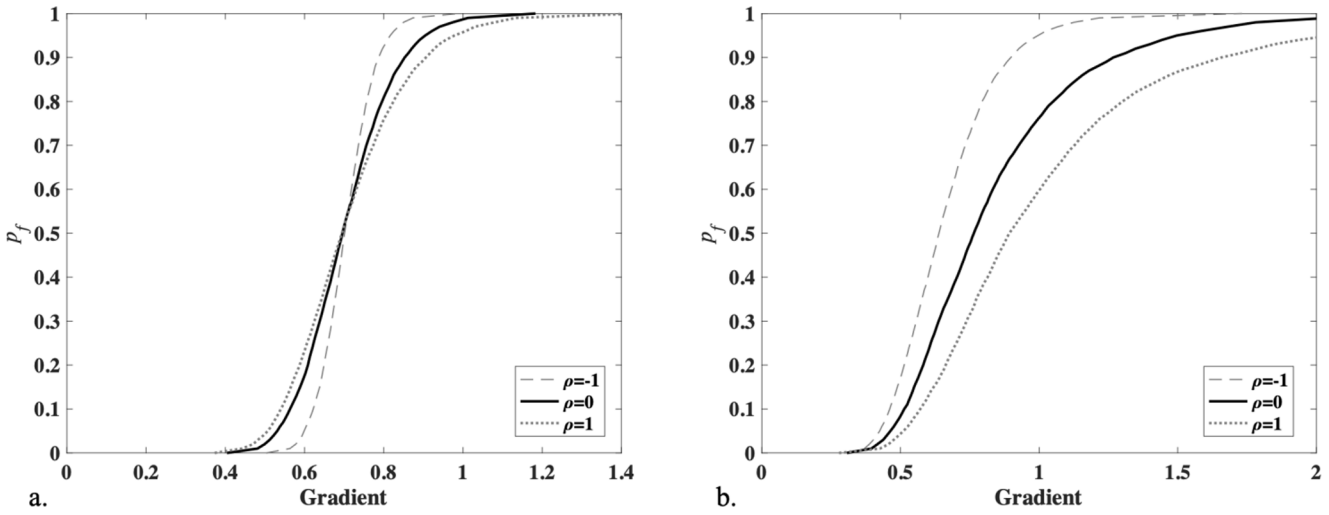

Fig. 15. Influence of correlation between i_{cr}-field and k-field on critical gradient distribution for (a) $\mu_k = 10^{-5}$m/s, σ_k/μ_k=0.25, θ/L=0.05, μ_{icr}=0.3, σ_{icr}=0.05 and (b) $\mu_k = 10^{-5}$m/s, $\sigma_k/\mu_k = 1.0$, θ/L=0.05, μ_{icr}=1.0, σ_{icr}=0.5.

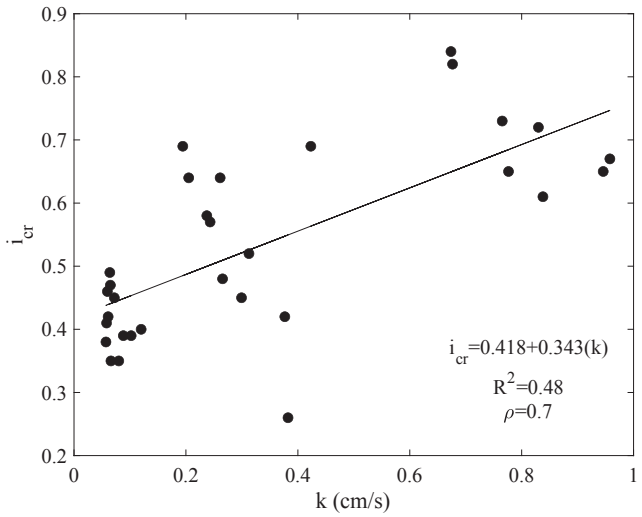

Fig. 16. Correlation between i_{cr} and k for uniformly graded sand based on lab measurements (Robbins et al. 2021).

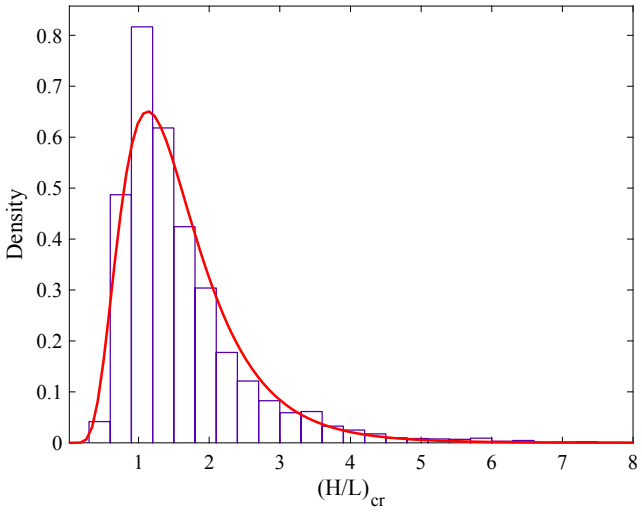

Fig. 17. Fit of lognormal distribution to Monte-Carlo results for scenario with $\mu_{icr} = 0.3$, σ_{icr}=0.15, ρ=0.

distribution parameters that resulted from the RFEM analysis. To assess the performance of the reduced order model at low probability values, Equations 10 and 11 were used to predict the distributions for all scenarios evaluated. The value of (H/L) associated with $p_f = 5\%$ obtained for each CDF using the reduced order model was then compared to the value obtained directly from the RFEM distributions (Fig. 18). While the reduced order model provides a reasonable representation of the RFEM results, there are errors of up to ±30% for many of the scenarios. As such, the authors recommend that the reduced order model only be used for understanding the general trends of the RFEM analysis results pending further study

4.3. Influence of initiation condition

In addition to investigating the influence of random soil properties on the distribution of $(H/L)_{cr}$, a series of analysis was conducted to determine the influence of the initiation condition on the probability of pipe progression. For the analyses discussed thus far, the erosion was initiated from a single element at the center of the downstream boundary. A few additional analyses were conducted in which the erosion was allowed to begin from any point along the downstream boundary. This was accomplished by switching every element on the downstream boundary to a pipe element simultaneously.

The resulting distribution obtained with initiation permitted along the entire boundary is compared to the case with initiation at a single point in Fig. 19 for one of the analysis cases. As seen, the CDF shifts to the left indicating that erosion is more likely when initiation can occur anywhere along the downstream boundary. Conceptually, this is explained by the fact that permitting initiation of erosion anywhere along the boundary ensures that the path of least resistance is followed during each realization. The low probability values of the CDF are for realizations in which the path of least resistance was already taken. Therefore, the lower portion of the CDF did not move. The upper portion of the CDF did shift, however, as the more resistant pipe paths followed when initiation was restricted to a single point were no longer followed. As a result, the hydraulic gradient required to cause piping decreased when erosion could be initiated anywhere on the boundary.

5. Conclusions

Backward erosion piping is a potential cause of failure in earth dams and levees that has been shown to be sensitive to variability in soil

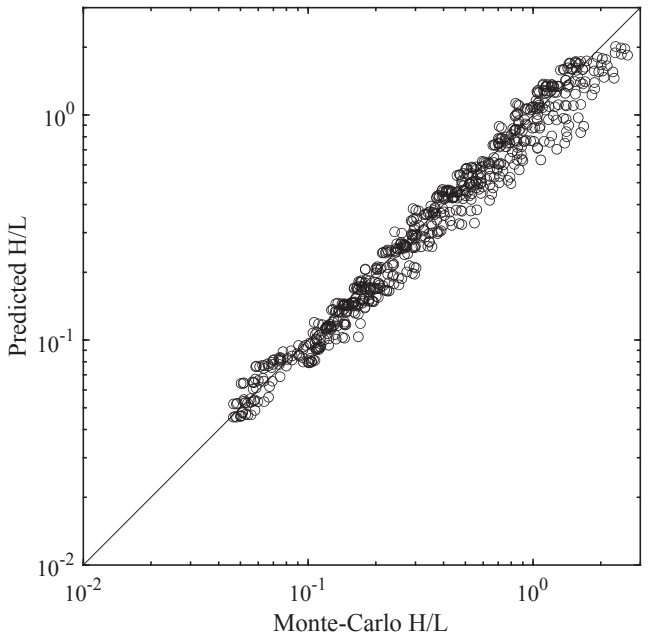

Fig. 18. Predicted $(H/L)_{cr}$ from reduced order model compared to $(H/L)_{cr}$ from Monte-Carlo results for $p_f = 5\%$.

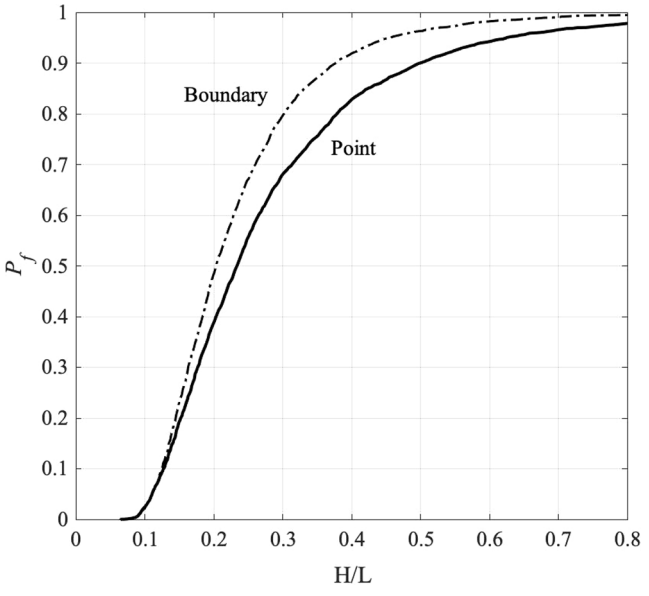

Fig. 19. Influence of initiation condition on resulting CDF.

properties. Numerical models for simulating piping developed to date have not included the option of statistically defined, spatially variable soil properties. This study developed and demonstrated a numerical approach for simulating BEP through spatially random soils using the Random Finite Element Method (RFEM). A finite element model for simulating BEP progression was used to simulate the progression of BEP erosion pipes through soils in which the hydraulic conductivity and critical hydraulic gradient for pipe progression were treated as random fields.

The results demonstrated that the probability of failure due to piping increases as the spatial correlation length increases. Additionally, any increase in hydraulic conductivity variance leads to increased resistance against piping for cases with small spatial correlation lengths. However, if the spatial correlation length is large, increased variance in the hydraulic conductivity leads to an increased probability of failure in the range of typical target reliabilities commonly assessed for dams and levees. Any increase in the mean value of the critical hydraulic gradient for pipe progression decreased the probability of failure due to pipe progression. On the contrary, any increase in the variance of the critical hydraulic gradient distribution made piping failure more likely.

The resulting distributions from the 700+ scenarios for which RFEM analyses were conducted were fitted to lognormal distributions in an attempt to develop a predictive model for the mean and standard deviation of the average hydraulic gradient needed to produce a given probability of BEP failure. Results indicate that the reduced order model is capable of representing the qualitative trends, albeit with up to 30% error in some instances. As such, the reduced order model at this time should be used only as a guide for indicating probabilistic trends in the RFEM results. Further work is needed to develop more accurate predictive models that might avoid the need for extensive RFEM studies whenever a new problem is encountered.

Finally, the influence of the initiation condition on the probability of BEP progression was also evaluated by conducting analyses in which erosion was allowed to initiate from any location on the downstream boundary as opposed to just one centrally located position. The results of these analyses indicate that the probability of failure increases for scenarios with unrestricted initiation locations as the weakest erosion path is readily followed for these scenarios.

While this study illustrates how RFEM may be used for analysis of BEP progression, significant research is needed before these techniques can be used for reliability analysis of dams and levees. In particular, the following limitations of the present study must be kept in mind when considering the results.

1. The two-dimensional, plan view formulation represents a 1-m thick sand bed. Further, the plan view calculations do not permit flow to pass below the pipe. In the field, a pipe may be only a few mm or cm in depth but passes through a sand bed of 10 m to 50 m in depth. As such, much of the flow in the real domain will not be conveyed towards this relatively small pipe, which may alter the influence the soil variability has on the results.
2. The pipe flow was assumed to be laminar. While this may be an appropriate assumption for fine sands (Robbins and Griffiths 2021), it may not be appropriate for higher k values present in some of the RFEM simulations with high σ_k.
3. BEP is a highly localized, three-dimensional, transient process that occurs over very large analysis domains (100–500 m). In this study, the process was assessed over a small, idealized domain with a simplified, two-dimensional, steady-state model to make the computational effort manageable.

Given these limitations, the results of this study should only be used in a qualitative manner to illustrate the general influence of spatial variability on the BEP process. Further research is needed to make RFEM suitable for assessing BEP in practice. In particular, research into appropriate constitutive relations, laboratory measured model parameters, and validation through analysis of case histories is greatly needed. Additionally, algorithmic development is needed in relation to adaptive mesh refinement strategies and techniques for reducing the cost of Monte-Carlo simulations. This will improve the ability to model localized phenomenon over larger problem domains. With these improvements, it will become feasible to implement three-dimensional models for more realistic assessment of BEP progression, and to better understand some of the limitations imposed by the assumptions made in the present study.

CRediT authorship contribution statement

B.A. Robbins: Conceptualization, Methodology, Software, Investigation, Writing - original draft. **D.V. Griffiths:** Methodology, Software,

Investigation, Writing - review & editing, Supervision. **Gordon A. Fenton:** Methodology, Software, Writing - review & editing.

Declaration of Competing Interest

The author declare that there is no conflict of interest.

Acknowledgements

This study was funded by the Flood and Coastal Research Program of the U.S. Army Corps of Engineers.

References

Allan, R., 2018. Backward erosion piping. PhD dissertation. Dept. of Civil and Environmental Engineering, University of New South Wales.
Baker, C., 2018. USACE conducts first analysis of risk and benefits of USACE levees. Flood Risk Management Newsletter (Vol. 11). Washington, D.C.
Bligh, W.G., 1910. Dams, barrages and weirs on porous foundations. Eng. Rec. 64 (26), 708–710.
Carrier III, W.D.C., 2003. Goodbye, Hazen; Hello, Kozeny-Carman. J. Geotech. Geoenviron. Eng. 129 (11), 1054–1056.
Clibborn, J., 1902. Experiments on the passage of water through sand. Govt. of India, Central Printing Office.
de Wit, J.M., 1984. Research Report on Sand Boil Model Tests. Delft, Netherlands.
Fascetti, A., Oskay, C., 2019. Dual random lattice modeling of backward erosion piping. Computers and Geotechnics, 105(May 2018), 265–276. https://doi.org/10.1016/j.compgeo.2018.08.018.
Fenton, G.A., 1994. Error evaluation of three random field generators. ASCE J. Eng. Mech. 120 (12), 2478–2497.
Fenton, G.A., Griffiths, D.V., 1993. Statistics of block conductivity through a simple bounded stochastic medium. Water Resour. Res. 29 (6), 1825–1830.
Fenton, G.A., Griffiths, D.V., 2008. Risk Assessment in Geotechnical Engineering. John Wiley & Sons.
Fenton, G.A., Vanmarcke, E.H., 1990. Simulation of random fields via local average subdivision. ASCE J. Eng. Mech. 116 (8), 1733–1749.
Foster, M., Fell, R., Spannagle, M., 2000. The statistics of embankment dam failures and accidents. Retrieved from Can. Geotech. J. 37 (10), 1000–1024. http://www.nrcresearchpress.com/doi/abs/10.1139/t00-030.
Fujisawa, K., Murakami, A., Nishimura, S., 2010. Numerical analysis of the erosion and the transport of fine particles within soils leading to the piping phenomenon. Soils Found. 50 (4), 471–482.
Griffiths, D.V., Fenton, G.A., 1993. Seepage beneath water retaining structures founded on spatially random soil. Géotechnique 43 (4), 577–587.
Hanses, U., 1985. The Mechanics of the Development of Erosion Pipes in a Layered Substratum Beneath Dams. Technischen Universitat Berlin.
Harr, M., 1962. Groundwater and Seepage. McGraw-Hill Inc.
Hoffmans, G., Van Rijn, L., 2018. Hydraulic approach for predicting piping in dikes. J. Hydraul. Res. 56 (2), 268–281. https://doi.org/10.1080/00221686.2017.1315747.
Kanning, W., Calle, E.O.F., 2013. Derivation of a representative piping resistance parameter based on random field modelling of erosion paths. Georisk: Assessment and Management of Risk for Engineered Systems and Geohazards, 7(2), 99-109.
Lane, E.W., 1935. Security from under-seepage masonry dams on earth foundations. Trans. ASCE 100 (1), 1235–1272.
Liang, Y., Yeh, T.C.J., Wang, Y.L., Liu, M., Wang, J., Hao, Y., 2017. Numerical simulation of backward erosion piping in heterogeneous fields. Water Resour. Res. 53 (4), 3246–3261.
Liu, K., Vardon, P.J., Hicks, M.A., 2017. Probabilistic analysis of seepage for internal stability of earth embankments. Environ. Geotechnics 1–13 (ahead of print).
Methorst, A.J., 2020. Piping in Sandy Tidal Deposits. Delft University of Technology.
Negrinelli, G., van Beek, V. M., Ranzi, R., 2016. Experimental and numerical investigation of backward erosion piping in heterogeneous sands. In Scour and Erosion (pp. 978–1).
Peitrus, T., 1981. An experimental Investigation of Hydraulic Piping in Sand. University of Florida.
Richards, K.S., Reddy, K.R., 2007. Critical appraisal of piping phenomena in earth dams. Bull. Eng. Geol. Environ. 66 (4), 381–402. https://doi.org/10.1007/s10064-007-0095-0.
Robbins, B.A., 2016. Numerical modeling of backward erosion piping. In: Proceedings of the 4th Itasca Symposium on Applied Numerical Modeling, (Itasca), 551–558.
Robbins, B.A., Griffiths, D.V., 2018. Modelling of Backward Erosion Piping in Two- and Three- Dimensional Domains. In: Bonelli, S., Jommi, C., Sterpi, D. (Eds.), Internal Erosion in Earth Dams, Dikes, and Levees. Springer Nature Switzerland AG, Cham, Switzerland, pp. 149–158. https://doi.org/10.1007/978-3-319-99423-9.
Robbins, B.A., Griffiths, D.V., 2021. A two-dimensional, adaptive finite element approach for simulation of backward erosion piping. Comput. Geotech. 129, 103820 https://doi.org/10.1016/j.compgeo.2020.103820.
Robbins, B.A., Griffiths, D.V., Fenton, G.A., 2019. Influence of Spatially Variable Soil Permeability on Backward Erosion Piping. In: Proceedings of the 7th International Symposium on Geotechnical Safety and Risk (ISGSR) (pp. 96–101). https://doi.org/10.3850/978-981-11-2725-0-bs2-cd.
Robbins, B.A., van Beek, V.M., Lopez-Soto, J., Montalvo-Bartolomei, A.M., Murphy, J., 2018. A novel laboratory test for backward erosion piping. Int. J. Phys. Modell. Geotechnics 18 (5), 266–279.
Robbins, B.A., Van Beek, V.M., 2015. Backward erosion piping: A historical review and discussion of influential factors. In: Association of State Dam Safety Officials, Dam Safety; 2015.
Robbins, B.A., Lucker, S., Griffiths, D.V., Van Beek, V., 2021. Progression of backward erosion piping in uniform sands. (In Review).
Rotunno, A.F., Callari, C., Froiio, F., 2019. A finite element method for localized erosion in porous media with applications to backward piping in levees. Int. J. Numer. Anal. Meth. Geomech. 43 (1), 293–316. https://doi.org/10.1002/nag.2864.
Schmertmann, J.H., 2000. The No-Filter Factor of Safety Against Piping Through Sands. In: Silva, F., Kavazanijian, E.J. (Eds.), Judgement and Innovation. American Society of Civil Engineers, pp. 65–133.
Schweckendiek, T., 2014. On Reducing Piping Uncertainties – A Bayesian Decision Approach. PhD Dissertation. Delft University of Technology.
Sellmeijer, J.B., 1988. On the mechanism of piping under impervious structures. Delft University of Technology.
Sellmeijer, J.B., 2006. Numerical computation of seepage erosion below dams (piping). International Conference on Scour and Erosion.
Sellmeijer, H., López, J., Cruz, D., van Beek, V.M., Knoeff, H., Van Beek, V.M., van Beek, V.M., 2011. Fine-tuning of the backward erosion piping model through small-scale, medium-scale and IJkdijk experiments. Eur. J. Environ. Civil Eng. 15 (8), 1139–1154. https://doi.org/10.3166/EJECE.15.1139-1154.
Shields, A., 1936. Anwendung der Ahnlichkeitsmechanik und Turbulenzforschung auf die Geschiebebewegung. Mitteilungen der Preußischen Versuchsanstalt für Wasserbau und Schiffbau. Berlin: heft 26. (In German).
Smith, I.M., Griffiths, D.V., 2004. Programming the finite element method, 4th ed. Wiley.
Terzaghi, K., Peck, R., 1948. Soil Mechanics in Engineering Practice. John Wiley and Sons.
Townsend, F., Bloomquist, D., Shiau, J.-M., Martinez, R., Rubin, H., 1988. Evaluation of filter criteria and thickness for mitigating piping in sands. Gainseville, Florida.
van Beek, V.M., 2015. Backward erosion piping: initiation and progression. Technische Universiteit Delft. https://doi.org/10.1007/s13398-014-0173-7.2.
van Beek, V., de Bruijn, H., Knoeff, J. G., Bezuijen, A., Förster, U., Beek, V. M. Van, & Bruijn, H. T. J. De. (2010). Levee Failure Due to Piping: A Full-Scale Experiment. In International Conference on Scour and Erosion (Vol. 2010, pp. 283–292). Delft, Netherlands: ASCE. Retrieved from http://link.aip.org/link/?ASCECP/392/27/1.
van Beek, V.M., Robbins, B.A., Hoffmans, G.J.C.M., Bezuijen, A., van Rijn, L.C., 2019. Use of incipient motion data for backward erosion piping models. Int. J. Sedim. Res. 34 (5), 401–408. https://doi.org/10.1016/j.ijsrc.2019.03.001.
van Beek, V. M., Yao, Q. L., & Van, M. A. (2013). Backward Erosion Piping Model Verification Using Cases in China and the Netherlands. In Seventh International Conference on Case Histories in Geotechnical Engineering (pp. 1–7). Chicago, IL.
Van Esch, J.M., Sellmeijer, J.B. & Stolle, D. 2013. Modeling Transient Groundwater Flow and Piping under Dikes and Dams. In 3rd International Symposium on Computational Geomechanics (ComGeo III), 9.
Vandenboer, K., 2019. A Study on the Mechanisms of Backward Erosion Piping. Ghent University.
Wang, D., Fu, X., Jie, Y., Dong, W., Hu, D., 2014. Simulation of pipe progression in a levee foundation with coupled seepage and pipe flow domains. Soils Found. 54 (5), 974–984. https://doi.org/10.1016/j.sandf.2014.09.003.
White, C.M. (1940). The equilibrium of grains on the bed of a stream. Proceedings of the Royal Society, 174(series A), 322–338.